ORIGINAL ARTICLE

Enhancement of weld strength of laser-welded joints of AA6061-T6 and TZM alloys via novel dual-laser warm laser shock peening

Gaurav V. Inamke[1] · Luca Pellone[1] · Jie Ning[1] · Yung C. Shin[1]

Abstract

In this paper, an experimental study is presented on an investigation to improve the weld strength of laser-welded joints via post-processing by warm laser shock peening (wLSP). A dual-laser setup was utilized to simultaneously heat the sample to a prescribed temperature and to perform the wLSP process on the laser-welded joints of AA6061-T6 and TZM alloys. Joints in overlap and bead-on-plate configurations were created by laser welding by a high-power fiber laser and post-processed with wLSP. The tensile tests carried out on wLSP-processed AA6061-T6 samples demonstrate an enhancement in the strength by about 20% over as-welded samples and the ductility of samples processed by wLSP improved by 30% over as-welded samples. The bead-on-plate (BOP) welds of TZM alloy processed with wLSP demonstrated an enhancement in strength by about 30% and the lap welds processed with wLSP demonstrated an increase in the joint strength by 22%. Finite element analysis revealed that the depth and magnitude of compressive stresses imparted by wLSP were greater than room temperature laser shock peening (rtLSP), which contributed to the enhancement of the joint strength for processed samples.

Keywords Warm laser shock peening · Laser welding · Strength improvement, · Al6061 · TZM

1 Introduction

Material joining techniques such as fusion welding and solid-state welding are widely used for producing products in industry. The various methods of joining metals together include, but are not limited to, resistance welding, tungsten inert gas welding, metal inert gas welding, electron beam welding, friction stir welding, and laser welding. While these processes have been in use for a very long time, with highly sophisticated equipment and advanced techniques already being used, there still remains a great difficulty in predicting and achieving the desired quality of welds. Welding is a complex process in which a weld joint undergoes thermal, mechanical, metallurgical, and microstructural changes. Evaporation of alloying elements, changes in chemical composition and microstructure of alloys, porosity and resultant residual stresses after welding significantly affect the quality of the welded joint. Compared to conventional welding methods such as tungsten inert gas (TIG) welding, metal inert gas (MIG) welding, and friction stir welding, laser welding offers advantages such as high weld speed, narrow heat-affected zones, better weld quality, and superior mechanical properties of weld joints [1]. Despite these advantages, when it comes to laser welding of difficult-to-weld materials such as aluminum alloys and molybdenum alloys, there still exists a need to improve the joint strength of laser-welded joints.

For laser-welded AA6061-T6 alloy, weld strength is a critical concern since there is a considerable drop in the material strength at the joint [2, 3]. Porosity is one of the primary reasons for the reduced mechanical strength of the welds [2] [3]. Padmanabham et al. [4] reported a joint strength of ~65% compared to that of the base metal for laser-welded bead-on-plate welds of AA6061-T6. Narsimhachary et al. [5] reported low hardness in the fusion zone of the weld specimens and a tensile strength of 197 ± 20 MPa for bead-on-plate laser-welded joints compared to the tensile strength of 300 MPa for the base metal. Chu et al. [6] investigated weld strength of laser-welded AA6061-T6 with filler material and reported joint strengths in the range of 94–107 MPa. El-Batahgy and Kutsuna [7] reported presence of porosity and solidification cracking in welded specimens of AA6061-T6. Hirose et al. [8] investigated the joint strength of laser-welded AA6061-T6 bead-on-plate welds and reported a weld

✉ Yung C. Shin
shin@purdue.edu

1   Center for Laser-Based Manufacturing, School of Mechanical Engineering, Purdue University, West Lafayette, Indiana, USA

Table 1 Chemical composition of the as-received AA6061-T6

Element	Si	Fe	Cu	Mn	Mg	Cr	Zn	Ti	Other	Al
Content %	0.69	0.43	0.22	0.13	0.87	0.16	0.04	0.02	0.03	Rem.

Table 2 Chemical composition of the as-received TZM Alloy

Element	Fe	Ni	Si	Ti	Zr	C	N	O	Mo
Content %	0.0007	0.0005	< 0.002	0.47	0.087	0.022	0.003	0.042	Rem.

Table 3 Material thickness for various welding configurations

Material	Welding configuration	Material thickness
AA6061-T6	Lap weld	1 mm
	BOP weld	2 mm
TZM alloy	Lap weld	0.5 mm
	BOP weld	1 mm

strength of about 70% compared to that of the base metal. The authors also processed the welds with post-weld aging and reported about 15% improvement in weld strength. Most earlier studies however mainly focused on bead-on-plate and butt-weld configurations. There has been less focus on the joint strength of laser-welded lap joints. Kim et al. [9] reported that partial penetration of lap-welded Al 5052 resulted in greater porosity. However, the strength of the welded joints was not reported. A recent study by Pellone et al. [10] reported that for laser-welded AA6061-T6 lap joints, the addition of an interface gap resulted in low porosity, good appearance, and strong lap welds.

TZM is a molybdenum-based alloy that has high strength at high temperatures, high thermal conductivity, high hardness,

and good corrosion resistance. Along with these properties, low neutron absorption cross-section and high recrystallization temperature make TZM particularly useful in nuclear power applications, as well as in the aerospace and defense industry. While TZM alloys exhibit excellent strength and toughness, welding of TZM alloys to construct functional structural components is particularly problematic. TZM welds are usually marred by high porosity, a loss of plasticity and brittle failure under loading, and a drastic reduction in joint strength. Chatterjee et al. [11] reported a welded joint strength of 41% and 47% to that of the base metal for electron beam welding (EBW) welds and laser-tungsten inert gas welds respectively. Stutz et al. [12] reported a weld strength of 50 to 77% that of the base metal for welds created by EBW. They also reported that the grains in the fusion zone and the heat-affected zone were coarse.

For the improvement of weld strength, post-weld treatments such as post-weld aging treatment [13], stress relief annealing heat treatment [14], cold rolling [15], and shot peening [16] have been implemented in the past. However, these methods have inherent limitations: post-weld aging treatment and stress relief annealing have very high processing time, and shot peening has low depth of compressive residual stresses as well as inability of treating all the areas

Fig. 1 Load vs displacement curves for heat-treated AA6061-T6 (left) and TZM alloy (right)
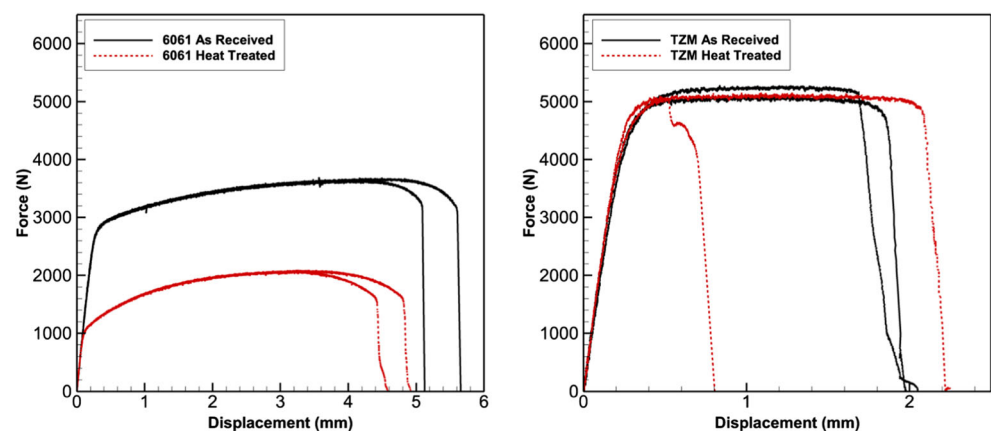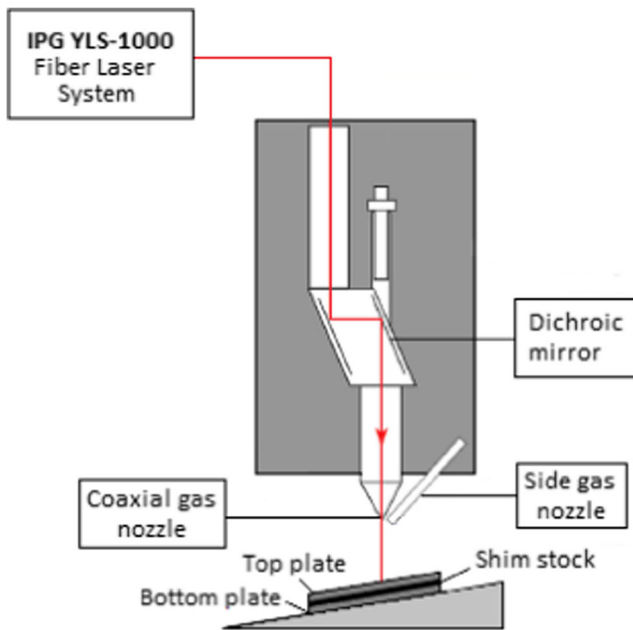
Fig. 2 Schematic diagram of the laser welding system

such as internal surfaces for parts with complex geometry. When applied to brittle materials like TZM, shot peening induces undesirable cracking into the material [17]. Laser shock peening (LSP) is a well-established process that imparts beneficial compressive residual stresses to a greater depth into the material, which can induce various benefits such as higher

fatigue life and higher stress corrosion resistance. The superior benefits of LSP as a post-weld treatment for laser-welded materials have been studied sparsely. Hatamleh et al. [16] reported that LSP as a post-welding treatment for friction stir-welded joints of Al 7075 and Al 2195 slowed down fatigue crack growth. Zhang et al. [18] reported a roughly 12% increase in the tensile strength of laser-welded ANSI 304 stainless steel joints after LSP. Chen et al. [19] observed grain refinement, higher dislocation density, increased hardness, elimination of tensile residual tensile stresses, and introduction of compressive residual stresses in the weld zone and heat-affected zone after LSP of Incoloy 800H laser-welded joints.

Precipitation hardened materials cause a "dislocation pinning" effect [20], which further enhances the ultimate tensile strength of the material. Precipitation hardening, which is a static aging process, however, is a time-consuming process that results in the formation of precipitates. On the contrary, dynamic aging leads to rapid formation of both precipitates and dislocations. Dynamic aging is a high-speed precipitation process that was first reported for 6000 series alloys by Roven et al. [21]. They reported formation of precipitates under severe plastic deformation via equal channel angular pressing at an elevated temperature of 175 °C. The generation of nanoscale precipitates by processing AA6061 with warm laser shock peening (wLSP) was reported by Ye et al. [22]. Highly dense nano-precipitates were reported by Liao et al. [20] when AA6061 was processed with warm LSP at elevated

Table 4   Welding parameters for Lap and BOP welds

Material	Plate thickness (mm)	Joint type	Laser power (W)	Welding Speed (m/min)	Interface gap (mm)	Shielding gas type	Alloy element
AA6061 -T6	1	Lap	1000	1.4	0.038	He	–
	2	BOP	1000	1.4	–	He	–
TZM alloy	0.5	Lap	850	1	0.09	Ar	0.05-mm thick Zr foil
	1	BOP	1000	0.5	–	Ar	–

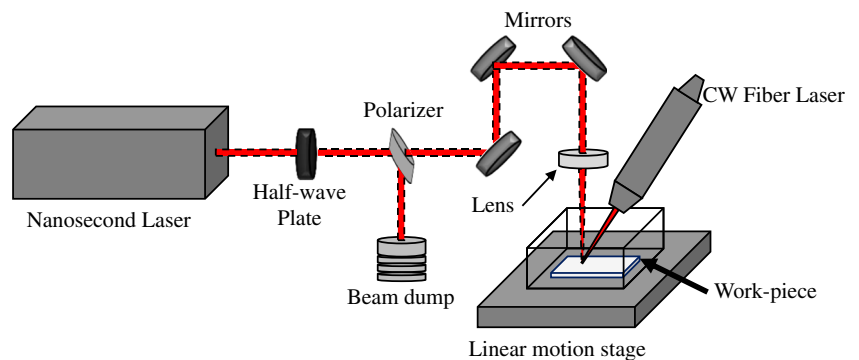Fig. 3 Schematic diagram of warm laser shock peening system

Fig. 4 Warm laser shock peening scheme for (left) laser welded lap joint and (right) laser welded bead-on-plate joint
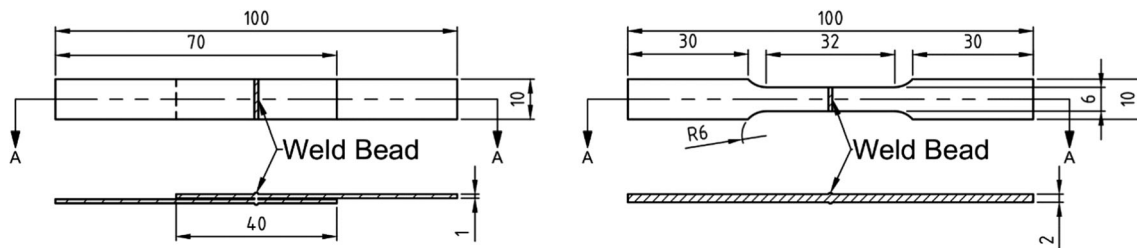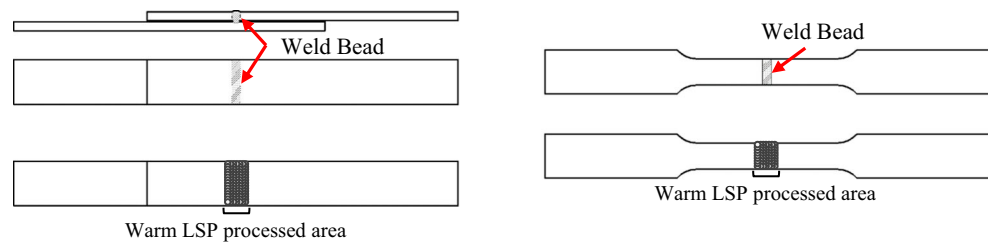

Fig. 5 Dimensions of tensile shear (left) and pure tensile (right) samples

Table 5 Thermal properties of AA6061-T6 and TZM alloy

Material	Density (kg/m^3)	Thermal conductivity (W/mK)	Specific heat (J/kgK)
Al 6061 [29]	2700	$164.11 + 3.58 \times 10^{-2}\ T + 2.0 \times 10^{-5}\ T^2$	$4087.1 - 17.231\ T + 1.02 \times 10^{-2}\ T^2$
TZM [30]	10,220	$119 - 4.46 \times 10^{-2}\ T + 2.26 \times 10^{-5}\ T^2$	$268 - 3.51 \times 10^{-2}\ T + 7.27 \times 10^{-5}\ T^2$

temperatures of 400–500 K. Ye et al. [23] investigated the effects of dense nano-precipitates and dislocations, generated by wLSP, on the strength and ductility of materials. Due to the obstacles provided by precipitates to dislocation movement, a dislocation pinning effect is induced in the materials processed with wLSP. This dislocation pinning effect provides enhanced resistance to dislocation movement, thereby increasing material strength and providing improved stability of residual compressive stresses in the material. The dislocation density generated by wLSP is lower than rtLSP, which leaves room for dislocation accumulation. Nanoscale precipitate particles act as dislocation motion barriers effectively suppressing dislocation dynamic recovery and improving dislocation accumulation capacity which helps improve material ductility [23]. A review article by Liao et al. [24] lists the various benefits of wLSP, viz., increased material strength, greater and deeper compressive residual stresses, improved

stability of compressive residual stresses, retention of ductility, and higher fatigue lift. Su et al. [25] reported higher fatigue life for TIG welded AA6061-T6 joints after LSP at an elevated temperature, compared to those with room temperature LSP. This is a very useful property desirable in welded joints. Also, the nanoscale precipitates would assist in enhancing the ultimate tensile strength of the welded joints. However, previous investigations into wLSP involved achieving desired temperatures using a heating pad, which is not a practical solution for industrial application of wLSP as a post-processing technique to enhance the weld strength of laser-welded joints.

AA6061-T6 and TZM alloys are two materials that are completely at far ends of the spectrum with respect to physical and mechanical properties and machinability. AA6061-T6 is a lightweight, easily machinable material, whereas TZM alloy is a highly dense, tough to machine high-strength alloy. As these alloys vastly differ in their properties, any post-

Table 6 Process parameters for validation of laser heating model

Material	Laser Power (W)	Angle of Incidence (deg)	Scanning Speed (mm/s)	Laser beam spot diameter (μm)
AA6061-T6	30	15	1.5	500

Fig. 6 Laser heating model validation results
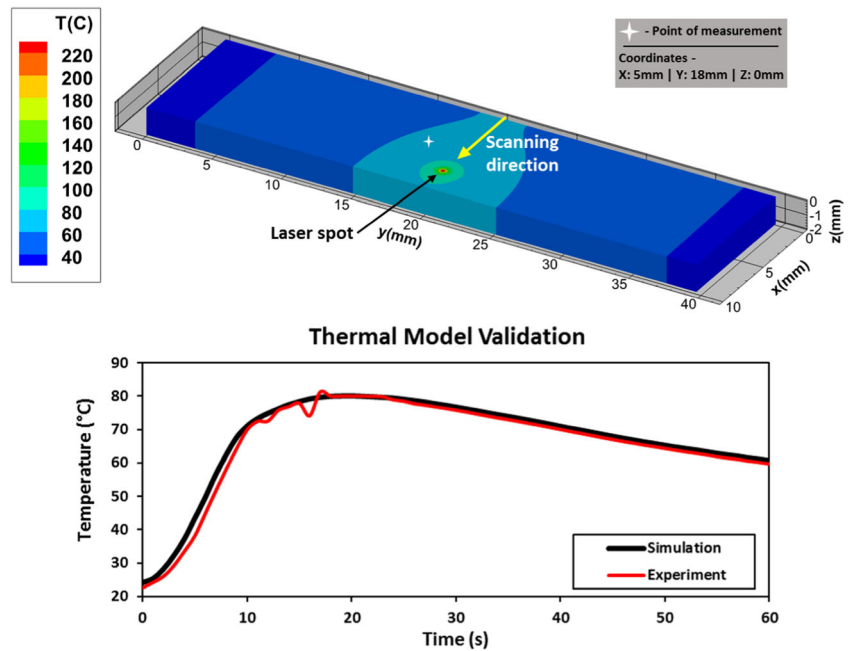
processing technique that produces improvement in mechanical performance of these alloys is a strong indicator of the merits of the post-processing technique. To establish the viability of *w*LSP as an effective post-processing technique for improving joint strength of laser-welded joints, AA6061-T6 and TZM alloy were chosen for this study. To investigate the effects of *w*LSP on the improvement of joint strength of laser-welded AA6061-T6 and TZM alloys, lap-welded joints and bead-on-plate (BOP)-welded joints were processed with *w*LSP using a novel dual-laser setup for rapid heating and laser shock peening and tested for mechanical performance. Finite element analysis of *w*LSP was carried out to understand the effects of warm temperature and silicone oil confinement based laser shock pressure on the residual stresses imparted into the material. This analysis was used to gain further insight into the improvement of joint strength of the welded joints.

2 Experimental setup and design

2.1 Laser welding

Rolled sheets of AA6061-T6 with a thickness of 1–2 mm and hot rolled TZM alloy sheets with a thickness of 0.5–1 mm were used in this study. Table 1 lists the composition of AA6061-T6, while Table 2 lists the composition of TZM alloy. Table 3 lists the thickness of materials used for different welding configurations. Prior to welding, the samples were ground using sandpapers to remove rough ridges and then cleaned with acetone to remove the oxide layer and any residual grease.

To evaluate whether pre-existing residual stresses affect material strength, AA6061-T6 and TZM alloy were heat treated with a stress relaxation annealing cycle per ASM standards [26]. Tensile testing was carried out on as received and heat-treated samples as per ASTM E8 standard. Figure 1 shows the load vs displacement curves for AA6061-T6 and TZM alloy processed with heat treatment. As the material strength dropped considerably in heat-treated AA6061-T6 and produced no significant improvement in heat-treated TZM alloy, it was determined that the pre-existing residual stresses do not affect the as-received material strength adversely. Therefore, heat treatment, which is an additional processing step, was discarded and as-received material was used for this study.
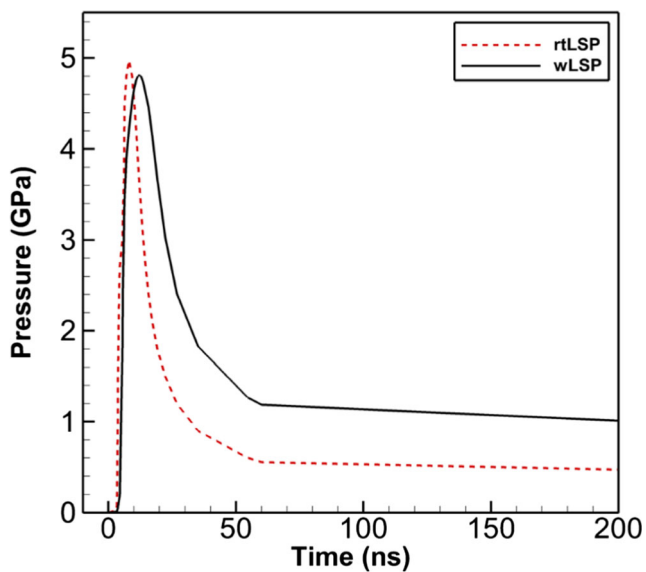

Fig. 7 Plasma pressure profile generated using a one-dimensional hydrodynamic model

Table 7 Material properties of AA 6061 T6 [34]

Material	E (GPa)	G (GPa)	v	ρ (kg/m^3)	T_m (°C)	Thermal expansion (10^{-6}/°C)	Thermal conductivity (W/m K)	Specific heat (J/kg K)
AA6061–T6	68.9	26	0.33	2700	582	23.6	167	896

Table 8 Johnson-Cook constitutive model parameters of Al 6061 T6 [33]

Material	A_{JC} (MPa)	B_{JC} (MPa)	n_{JC}	C_{JC}	m_{JC}	T_{ref} (°C)	T_m (°C)	$\dot{\varepsilon}_0$ (1/s)
AA6061–T6	324.0	114.0	0.42	0.002	1.34	25	582	1

All welding experiments were performed with an IPG YLR-1000 fiber laser (wavelength, 1077 nm) with a laser spot diameter of 240 μm and a circular Gaussian beam profile. The maximum power of the laser is 1000 W. During welding, the laser beam was inclined by 10° to protect the laser beam delivery optics from the induced plasma and splatter. Shim stocks were used to introduce and maintain the interface gap while clamping workpieces on the work surface. Argon or helium was used as the shielding gas for the top surface via side and coaxial nozzles and for the bottom surface via another nozzle. Lap welding experiments were conducted in keyhole welding mode where irradiation by a high-intensity laser causes simultaneous melting and evaporation of the weld pool via multiple reflections creating high pressure and a thermo-capillary effect that assist in deeper penetration of welds with a small heat-affected zone. For BOP welding, the setup is the same as that in lap welding except for the setup of the work-pieces. While in lap welding, the two plates being welded are stacked on top of each other with a shim stock in between (to introduce an interface gap) and then clamped to the workpiece holder, for bead-on-plate joints, a single plate is directly clamped onto the workpiece holder. The schematic diagram

of the laser welding system is shown in Fig. 2. Welding parameters for AA6061-T6 and TZM alloys are listed in Table 4.

2.2 Warm laser shock peening

Warm laser shock peening (wLSP) experiments were carried out using the experimental setup shown in Fig. 3. An Nd-YAG laser beam with a wavelength of 1064 nm and a pulse duration of 6 ns was focused onto the top surface of the workpiece to perform LSP, after passing through a half wave plate, a thin film polarizer, three high reflecting mirrors, and a focusing lens. The focused laser beam diameter on the surface of the workpiece can be changed by varying the distance between the workpiece and the focusing lens. A secondary continuous wave fiber laser (IPG YLR 150/1500 QCW) was focused on the surface of the workpiece such that it coincides with the laser spot of the Nd-YAG laser. The fiber laser was used to locally heat the workpiece to 425–500 K to bring it into the warm LSP regime. The workpiece was placed in a tank filled with a high-temperature silicone fluid (with a flash point of 590 K) to produce a fluid confinement regime. The samples used in this work were laser-welded AA6061-T6 and TZM
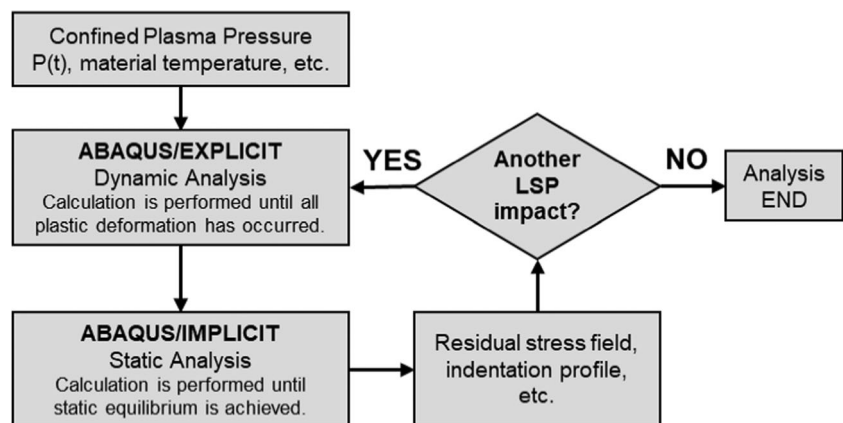
Fig. 8 FEM calculation procedure

Fig. 9 BOP samples **a** processed with wLSP **b** on top and bottom surface
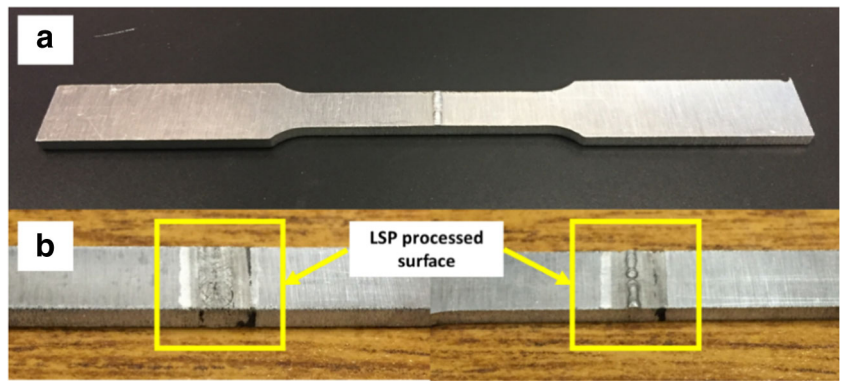

Table 9 Parameters of rtLSP and *w*LSP used to process BOP samples

Type of LSP	Coating layer	Confinement layer	Workpiece temperature (K)	Laser power density (GW/cm^2)	Peening overlap ratio
Room temperature LSP (rtLSP)	50-μm thick black paint	Water	300	7	50%
Warm LSP (wLSP)	50-μm thick aluminum foil	High-temperature silicone oil	425–500	7	50%

Fig. 10 a Ultimate tensile strength and **b** elongation of specimen at failure for BOP-welded samples of as-welded, processed with rtLSP, and wLSP
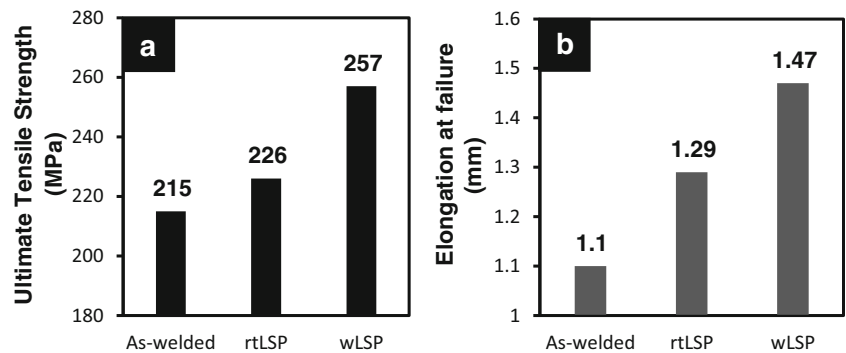

Fig. 11 a Load vs. displacement curves for tensile testing of BOP samples and **b** tensile-shear testing of lap-welded samples
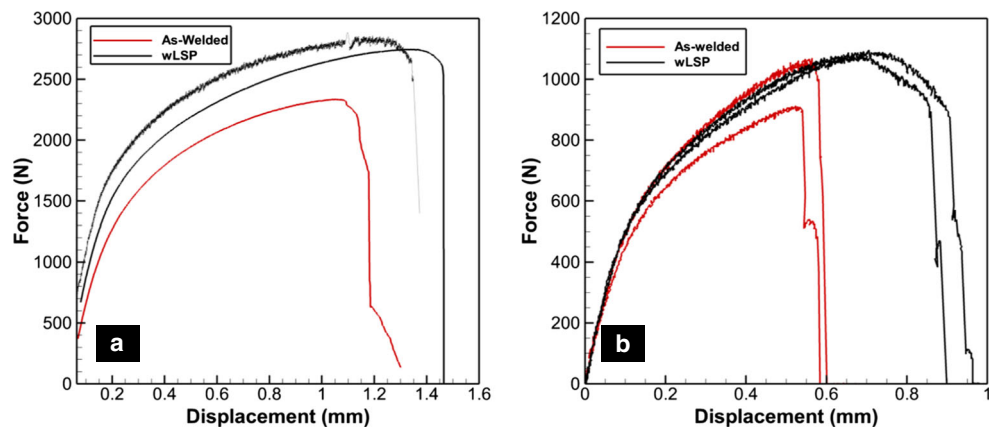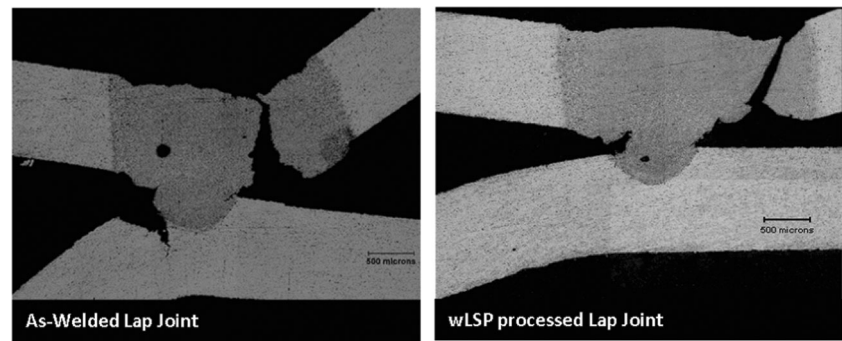
Fig. 12 Failure modes for Al 6061 lap joints without and with wLSP

alloy lap joints and BOP joints. Aluminum foil of thickness 50 μm was employed as the sacrificial layer, which was bonded to the welded samples with a very thin layer of silicone gel. The laser power density of the ns-laser was 7 GW/cm^2 and the overlap ratio of multitrack laser shock peening was 50%. The tank containing the sample was moved on a motorized table to perform multitrack laser shock peening over the weld region as shown in Fig. 4. In overlap configuration joints, the top surface of the top plate and the bottom surface of the bottom plate were processed with wLSP. For BOP configuration joints, the top and bottom surfaces along the weld were processed with wLSP. A non-contact 3D optical profiler was used to measure the indentation depths of samples processed with rtLSP and wLSP.

2.3 Mechanical testing

Tensile shear and cross tension tests for lap-welded joints as well as tensile tests for bead-on-plate welded joints were carried out on an MTS 858 Mini Bionix machine. The testing
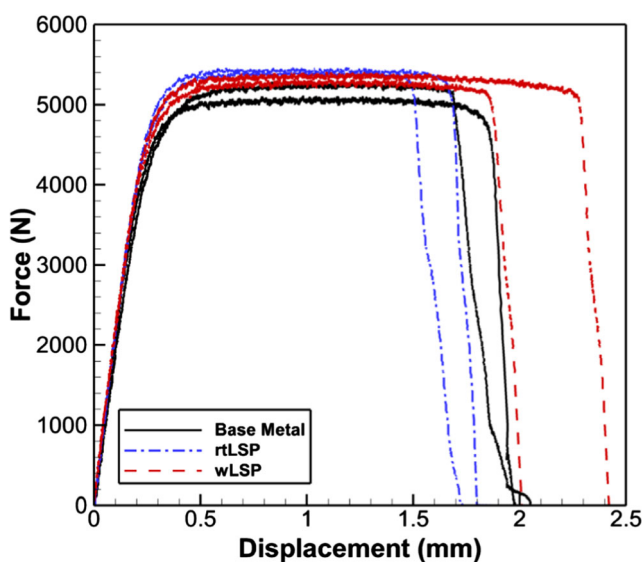

Fig. 13 Load-displacement curves for as-received TZM alloy processed with rtLSP and wLSP

speed was determined by a constant displacement rate of 0.5 mm/min for each sample. The tensile shear and tensile tests were carried out per ASTM E8 standard and cross tension tests were carried out per ISO 14272 standard. In order to prepare the testing samples with dimensions shown in Fig. 5, a Flow Mach 22020c water jet machine was used.

2.4 Modeling of warm laser shock peening

2.4.1 Laser heating model

Warm laser shock peening is a thermally engineered process, i.e., control of temperature in the workpiece is critical to ensure that it is in the dynamic strain aging and dynamic precipitation regime. Therefore, in this study, it was critical to determine the average power of the heating laser that would locally heat the material to temperatures in range of 400–500 K. A three-dimensional transient heat transfer model for laser heating based on the finite element method, developed by Tian and Shin [27], was utilized to predict the temperature in the target material. The model has been previously utilized to predict surface temperatures for a variety of materials such as Ti-6Al-4V, Inconel, Iron, etc.

AA6061-T6 is a highly reflective material to the light of wavelength 1064 nm with 80% of normally incident light reflected off its surface [28]. To avoid damage to the optical elements of the fiber laser, the angle of incidence of the heating laser was set to 15° and this was incorporated in the thermal model. The laser beam spot diameter of the heating laser was set at 500 μm to coincide with the spot diameter of the pulsed laser. Thermal properties of AA6061-T6 and TZM alloy used for the laser heating modeling are listed in Table 5. For validating the temperature predicted using the thermal model, laser heating experiments were carried out with the sample process parameters as the simulation and the evolution of temperature at a point adjacent to the scanning line was obtained from the simulation and experiment and compared. In order to measure the temperature of the material at the point of measurement, a thermocouple was embedded into the material and sealed from the outside environment with thermal cement. A data acquisition system was used to capture the

Fig. 14 Load vs displacement curves for **a** tensile testing of BOP samples and **b** tensile-shear testing of lap-welded samples
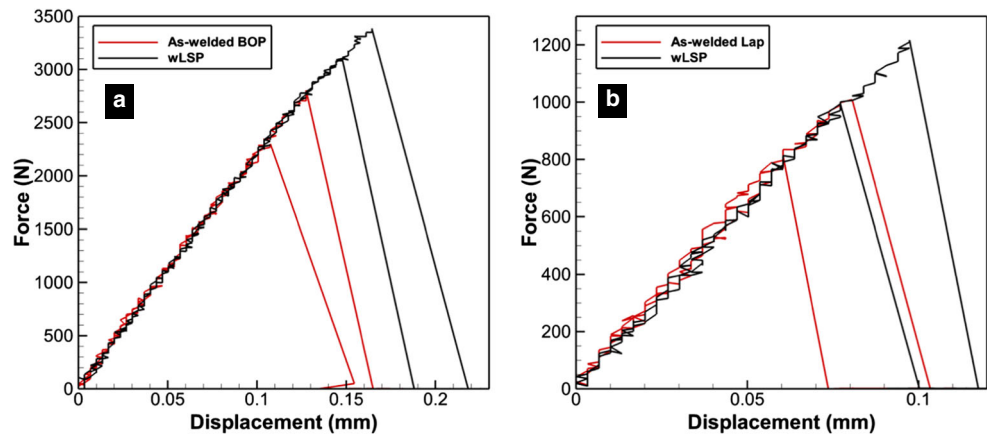
temperature measurements. Process parameters used for experimental validation of the laser heating model are listed in Table 6.

Figure 6 shows the evolution of temperature at a predefined location on the material as well as the peak temperature predicted by the laser heating model. The peak temperature reached by the laser is within the wLSP range despite the average laser power being as low as 30 W. This is due to the high power density of 15.3 kW/cm^2 that was generated by irradiating a focused laser beam onto the surface of the material. The predicted temperature values also agree with the experimentally measured temperature values. Once the thermal model was validated, it was utilized to determine the laser power required to heat the target material to a required temperature.

2.4.2 Confined plasma model

The one-dimensional confined plasma model developed earlier by Wu and Shin [31] was used to calculate the plasma pressure generated during wLSP in an oil confinement regime and during rtLSP in a water confinement regime. As the laser beam diameter was 500 μm (larger than critical diameter of 300 μm), the two-dimensional effects of plasma expansion could be considered negligible and the one-dimensional

assumption was valid as demonstrated by Wu and Shin [32]. Figure 7 shows the plasma pressure predicted by this model for a laser beam of 6 ns and full width at half maximum (FWHM) at 7 GW/cm^2 power density with a 50-μm aluminum foil (wLSP) and black paint (rtLSP) on the AA6061-T6 substrate. From Fig. 7, it can be seen that the plasma pressure sustains for a longer duration in wLSP compared with rtLSP.

2.4.3 3D finite element model

A 3D finite element model was developed to utilize the plasma pressure as input and calculate the shock wave propagation and obtain resultant residual stresses in the substrate material. For the laser shock peening process, the typical strain rate is as high as 10^7 s^{-1}, and as a result, the dynamic yield strength of the material is considerably increased due to work hardening and strain-rate hardening. Therefore, capturing the dynamic behavior of the target material is critical in simulating the residual stresses in the material. The dynamic behavior of AA6061-T6 was described by the Johnson-Cook constitutive model [33],

$$\sigma = \left(A_{JC} + B_{JC}\varepsilon^{n_{JC}}\right)\left(1 + C_{JC}ln\left(\frac{\dot{\varepsilon}}{\dot{\varepsilon}_0}\right)\right)\left(1 - \left(\frac{T - T_{ref}}{T_m - T_{ref}}\right)^{m_{JC}}\right)$$

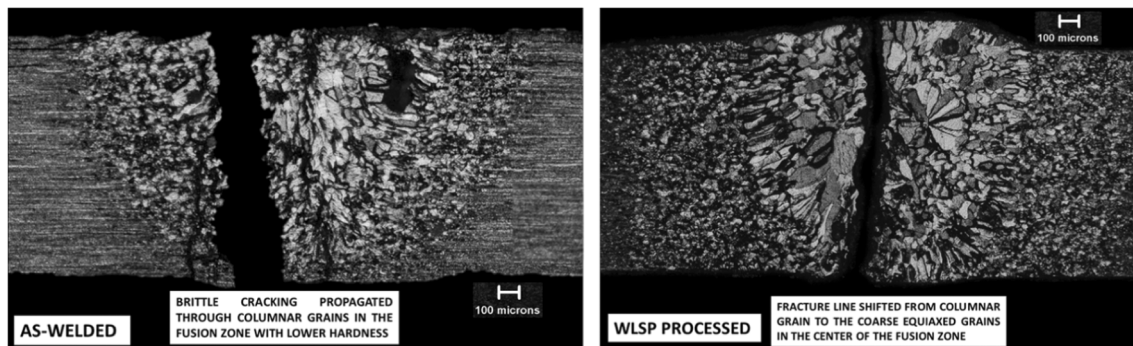with the material properties and Johnson-Cook constitutive model parameters listed in Tables 7 and 8.

Fig. 15 Failure modes for TZM alloy BOP joints without (left) and with wLSP (right)
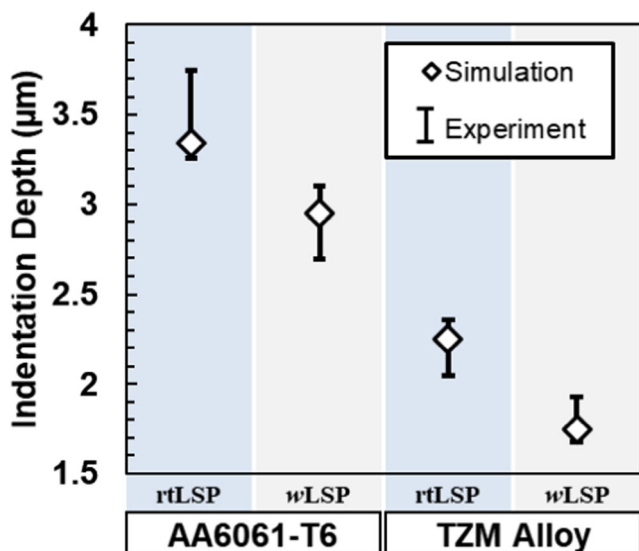
Fig. 16 Indentation depth comparison for simulation and experimental data. (rtLSP—coating: black paint, overlay: water, material temperature: 296 K) (wLSP—coating: Al foil, overlay: silicon oil, material temperature: 500 K) (laser power density: 7GW/cm^2)

To calculate the dynamic propagation of the shock wave through the material as well as residual stress state, a combined FEM calculation procedure with ABAQUS/EXPLICIT and ABAQUS/STANDARD was employed as shown in Fig. 8.

3 Results and discussion

3.1 wLSP of AA6061-T6-welded joints

Lap-welded and BOP-welded samples of AA6061-T6 were processed with wLSP. A sample BOP joint that has been processed by wLSP is shown in Fig. 9. To evaluate the benefits of wLSP over conventional room temperature LSP (rtLSP), BOP

samples were first processed with rtLSP and wLSP. Table 9 lists the parameters used for rtLSP and wLSP. Tensile testing of LSP processed samples exhibited higher strength than those of as-welded samples. Figure 10 shows the ultimate tensile strength and the elongation to failure for BOP samples in three test conditions viz. "as-welded," "as-welded + rtLSP" and "as-welded + wLSP." From Fig. 10a, it can be seen that wLSP improves the tensile strength of welded joint by about 20%. Also, Fig. 10b shows that there is a significant improvement in ductility of wLSP-processed samples. The mechanisms that cause this improvement in strength and ductility are discussed in detail later in this section.

Due to the significant advantage obtained by processing welded samples with wLSP, all the BOP- and lap-welded joints of AA6061-T6 and TZM were subsequently processed only with wLSP. Figure 11 shows the load-displacement curves for AA6061-T6 when processed with wLSP.

As illustrated by the tensile load-displacement curve in Fig. 11a, the samples processed with wLSP sustained higher loads than as-welded samples. Dynamic precipitation caused by wLSP led to the creation of dislocations and nano-precipitates in the material. During tensile loading, the nano-precipitates acted as barriers to the dislocation movement. This dislocation pinning effect led to the improved material strength and higher maximum load carried by the weld. It was also observed that the ductility of samples processed with wLSP is higher than that of as-welded samples. This beneficial effect can be attributed to the combination of nanoscale precipitates and the lower dislocation density caused by the elevated temperature during wLSP processing of welded samples, which aided in improved dislocation accumulation capacity. Figure 11b shows the tensile shear load-displacement curve for the lap joint samples processed with wLSP, which shows that wLSP-processed lap joints sustained slightly higher loads under tensile shear loading, but a significant improvement in ductility. Figure 12 displays the failure modes of the as-welded and wLSP processed lap-welded joints tested under tensile loading. An inspection of

Fig. 17 Residual stress prediction for **a** AA6061-T6 and **b** TZM alloy
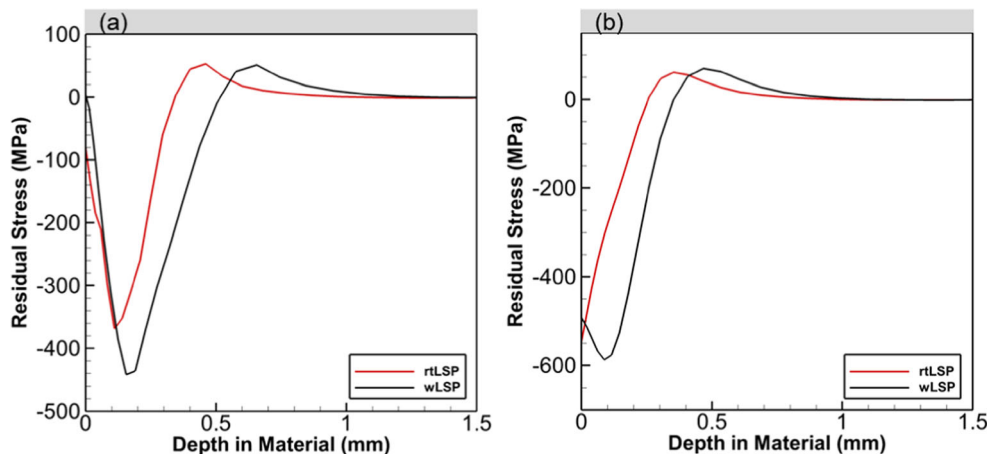
failure mode for the tensile shear samples revealed crack initiation and propagation occurred in the heat-affected zone for all the samples. As shown in Fig. 12, wLSP-processed samples exhibited lower deformation of the top and bottom plates than that of as-welded samples. Crack initiation and propagation in the bottom plate was restricted in wLSP samples compared to as-welded samples.

3.2 wLSP of TZM alloy welded joints

TZM alloys have been very scarcely studied in the past, and to the best knowledge of the authors, there are no studies on the effects of laser shock peening on TZM alloys. Therefore, to develop a baseline on the impact that rtLSP and wLSP have on TZM alloys, as-received, TZM alloy samples were processed with rtLSP and wLSP and then tensile testing was carried out. Figure 13 illustrates the load-displacement curves for tensile testing of three conditions, viz. base metal, base metal + rtLSP, and base metal + wLSP.

As shown in Fig. 13, processing TZM with rtLSP induced beneficial compressive stresses, thereby slightly increasing the tensile strength of the material. However, a loss of ductility was observed, which resulted in lower elongation in rtLSP-processed material at failure. On the other hand, wLSP enhanced both the tensile strength and ductility of the material. Subsequently, BOP-welded and lap-welded joints of TZM alloy were processed only with wLSP and the load-displacement curves are displayed in Fig. 14.

Welded TZM alloys lose plastic behavior and are embrittled, resulting in much lower strength than the base material as reported in previous studies [11, 12]. As shown in Fig. 14, the as-welded samples display no plastic behavior and lose a significant portion of tensile strength. The BOP joints processed with wLSP displayed an increase in tensile strength by an average of 30% compared to as-welded BOP joints. Failure modes for BOP-welded joints are shown in Fig. 15. The failure in as-welded samples propagated through the columnar grain zone which moved to the coarse equiaxed region in the wLSP-processed joints [35]. Lap joints processed with wLSP exhibited an increase in strength by a similar amount compared to as-welded lap joints. Failure mode inspection for the tensile shear samples processed with wLSP revealed crack initiation in the interface region of the weld and propagation towards the center of the weld in the top plate. The wLSP induced dynamic strain aging [36] and dynamic precipitation [37], which result in dense nano-precipitates, causing a dislocation pinning effect, which was the underlying mechanism that resulted in increased loads sustained by lap welds processed with wLSP.

3.3 Residual stresses induced in the welded joints

Cao et al. [38] combined the confined plasma model [24] developed in the authors' group with a 3D finite element model, and accurately predicted the indentation depth and residual stresses for various materials with good agreement with experimental data. Therefore, in this study, indentation depth predicted by simulations were compared with experimental data for rtLSPed- and wLSPed-welded joints. Figure 16 shows the comparison of indentation depths predicted and measured for rtLSP and wLSP processed AA6061-T6 and TZM alloys. As the predicted indentation depths were found to be in good agreement with experimental data, the residual stresses predicted were deemed to be accurate.

Residual stresses predicted by the finite element model are shown in Fig. 17. As can be seen in Fig. 17, the magnitude as well as depth of the compressive residual stresses are higher in wLSP samples than in the rtLSP-processed samples. This prediction is in good agreement with previous findings on residual stresses induced by wLSP [20, 25].

The maximum compressive residual stress induced by wLSP in AA6061-T6 is about 440 MPa in magnitude and in TZM alloy is about 600 MPa in magnitude. The compressive zone depth in the wLSPed part is greater than in the rtLSPed part. The deeper residual stresses after wLSP can be attributed to the elevated temperature of the material along with a more sustained shock pressure (refer to Fig. 7). The deep residual stresses in combination with nano-precipitates generated by dynamic strain aging can contribute to higher residual stress stability under cyclic loading, and consequently increased fatigue life of the material.

These predictions of residual stresses are for base metal; welded joints may have tensile residual stresses existing in the joint region. Therefore, the welded samples in this study were subjected to stress-relaxation annealing to measure the impact of pre-existing tensile stresses on the joint strength. However, there was no significant increase in joint strength after stress-relaxation annealing, indicating that the joint strength was not impacted adversely by pre-existing tensile stresses. It can, therefore, be safely assumed that even for welded joints, the prediction of compressive residual stresses is valid.

4 Conclusions

(1) Warm laser shock peening was an effective method of increasing joint strength of laser-welded joints, which is known to be a critical area for improvement. The use of a novel dual-laser setup for rapid heating and simultaneous wLSP is an industrially viable processing technique and can be used to rapidly improve the weld strength of in situ welded joints.

(2) The tensile strength of BOP welded AA6061-T6 alloy processed with *w*LSP was improved by about 20% and the ductility was improved by about 33%.

(3) Warm LSP improved the ductility of lap-welded AA6061-T6 joints by about 40%. While the failure mode occurred in the HAZ for both the as-welded and *w*LSP-processed samples, the dislocation pinning effect and pre-existing stress relaxation by *w*LSP contributed to the improved ductility.

(4) The tensile strength of BOP-welded TZM alloy processed with *w*LSP was improved by about 30% and the weld strength of lap-welded TZM alloy processed with *w*LSP was improved by about 22%.

(5) Finite element simulations showed deeper compressive residual stresses having a greater magnitude with *w*LSP compared to those of rtLSP. This increased depth of high magnitude compressive stresses assisted in the enhancement of strength of *w*LSP-processed laser-welded joints.

References

1. Hong K-M, Shin YC (2017) Prospects of laser welding technology in the automotive industry: a review. J Mater Process Technol 245:46–69

2. He E, Liu J, Lee J, Wang K, Politis DJ, Chen L, Wang L (2018) Effect of porosities on tensile properties of laser-welded Al-Li alloy: an experimental and modeling study. Int J Adv Manuf Technol 95(1–4):659–671

3. Mugica GW, Tovio DO, Cuyas JC, Gonzales AC (2004) Effect of porosity on the tensile properties of low ductility aluminum alloys. Mater Res 7(2):221–229

4. Padmanabham G, Shanmugrajan B (2009) Experimental investigation of bead-on-bead CO2 laser welding of Al alloy 6061. Trends in welding research, Proceedings of the 8th international conference, pp. 598–603

5. Narsimhachary D, Bathe RN, Padmanabham G, Basu A (2014) Influence of temperature profile during laser welding of aluminum alloy 6061 T6 on microstructure and mechanical properties. Mater Manuf Process 29(8):948–953

6. Chu Q, Bai R, Jian H, Lei Z, Hu N, Yan C (2018) Microstructure, texture and mechanical properties of 6061 aluminum laser beam welded joints. Mater Charact 137:269–276

7. El-Batahgy, A Kutsuna, Muneharu. (2009). Laser beam welding of AA5052, AA5083, and AA6061 aluminum alloys. Advances in Materials Science and Engineering. https://doi.org/10.1155/2009/974182

8. Hirose A, Kobayashi KF, Todaka H (1997) CO2 laser beam welding of 6061-T6 aluminum alloy thin plate. Metall Mater Trans A Phys Metall Mater Sci 28(12):2657–2662

9. Kim JK, Lim HS, Cho JH, Kim CH (2008) Weldability during the laser lap welding of Al 5052 sheets. Arch Mat Sci Eng 31(2):113–116

10. Pellone L, Inamke G, Hong KM, Shin YC (2019) The effects of interface gap and shielding gas on the welding quality during fiber laser lap welding of AA6061-T6. J Mater Process Technol 268:201–212

11. Chatterjee A, Kumar S, Tewari R, Dey GK (2016) Welding of Mo-based alloy using electron beam and laser-GTAW hybrid welding techniques. Metall Mater Trans A Phys Metall Mater Sci 47(3):1–10

12. Stutz M, Oliviera D, Ruttinger M, Reheis N, Kestler H, Enzinger N (2016) Electron beam welding of TZM sheets. Mater Sci Forum 879:1865–1869

13. Elangovan K, Balasubramanian V (2008) Influences of post-weld heat treatment on tensile properties of friction stir-welded AA6061 aluminum alloy joints. Mater Charact 59(9):1168–1177

14. Cheng X, Fisher JW, Prask HJ, Gnaeupel-Herold T, Yen BT, Roy S (2003) Residual stress modification by post-weld treatment and its beneficial effect on fatigue strength of welded structures. Int J Fatigue 25(9–11):1259–1269

15. Casalino G, El Mehtedi M, Forcellese A, Simoncini M (2018) Effect of cold rolling on the mechanical properties and formability of FSWed sheets in AA5754-H114. Metals 8(4):223

16. Hatamleh O, Lyons J, Forman R (2007) Laser and shot peening effects on fatigue crack growth in friction stir welded 7075-T7351 aluminum alloy joints. Int J Fatigue 29:421–434

17. Pfeiffer W, Wensel J (2010) Shot peening of brittle materials - status and outlook. *Mater Sci Forum* 638–642:799–804

18. Zhang L, Luo KY, Lu JZ, Zhang YK, Dai FZ, Zhong JW (2011) Effects of laser shock processing with different shocked paths on mechanical properties of laser welded ANSI 304 stainless steel joint. Mater Sci Eng A 528(13–14):4652–4657

19. Chen X, Wang J, Fang Y, Madigan B, Xu G, Zhou J (2014) Investigation of microstructures and residual stresses in laser peened Incoloy 800H weldments. Opt Laser Technol 57:159–164

20. Liao Y, Ye C, Gao H, Kim B-J, Suslov S, Stach EA, Cheng GJ (2011) Dislocation pinning effects induced by nano-precipitates during warm laser shock peening: dislocation dynamic simulation and experiments. J Appl Phys 110(2):023518

21. Roven HJ, Liu M, Werenskiold JC (2008) Dynamic precipitation during severe plastic deformation of an Al–Mg–Si aluminium alloy. Mater Sci Eng A 483-484:54–58

22. Ye C, Liao Y, Cheng GJ (2010) Warm laser shock peening driven nanostructures and their effects on fatigue performance in aluminum alloy 6160. Adv Eng Mater 12(4):291–297

23. Ye C, Liao YL, Suslov S, Lin D, Cheng GJ (2014) Ultrahigh dense and gradient nano-precipitates by warm laser shock peening for combination of high strength and ductility. Mater Sci Eng A 609(15):195–203

24. Liao Y, Ye C, Cheng GJ (2016) [INVITED] a review: warm laser shock peening and related laser processing technique. Opt Laser Technol 78(A):15–24

25. Su C, Zhou J, Meng X, Huang S (2016) Improvement in fatigue performance of aluminium alloy welded joints by laser shock peening in a dynamic strain aging temperature regime. Materials 9(10):799

26. Totten GE (2016) Heat treating of nonferrous alloys. In: ASM Handbook, vol 4E. ASM International, Materials Park

27. Tian Y, Shin YC (2005) Thermal modeling for laser-assisted machining of silicon nitride ceramics with complex features. J Manuf Sci Eng 128(2):425–434

28. Paquin RA (2010) Properties of metals. In: Handbook of optics, vol. IV: optical properties of materials, nonlinear optics, quantum optics. McGraw-Hill, New York

29. Touloukian YS (1966) Thermophysical and Electronic Properties Information Analysis Center Lafayette IN, recommended values of the thermophysical properties of eight alloys, major constituents and their oxides, Ft. Belvoir Defense Technical Information Center. http://www.dtic.mil/docs/citations/ADA952890

30. Smith D (1991) International Atomic Energy Agency, ITER blanket, shield and material data base. International Atomic Energy Agency, Vienna

31. Wu B, Shin YC (2005) A self-closed thermal model for laser shock peening under the water confinement regime configuration and comparisons to experiments. J Appl Phys 97(11):113517

32. Wu B, Shin YC (2007) Two dimensional hydrodynamic simulation of high pressures induced by high-power nanosecond laser-matter interactions under water. J Appl Phys 101:103514

33. Johnson GR, Cook WH (1983) A constitutive model and data for metals subjected to large strains, high strain rates and high temperatures. Proceedings of the Seventh International Symposium on Ballistics, The Hague, The Netherlands, pp. 541–547

34. Lampman S (1990) Metallography and microstructures. ASM Handbook , ASM International, Materials Park, Ohio.

35. Ning J, Hong KM, Inamke GV, Shin YC, Zhang L (2019) Analysis of microstructure and mechanical strength of lap joints of TZM alloy welded by a fiber laser. J Manuf Process 39:146–159

36. Filacchioni G, Casagrande E, De Angelis U, De Santis G, Ferrera D (2002) Effects of strain rate on tensile properties of TZM and Mo-5% Re. J Nucl Mater 307-311(1):705–709

37. Wilcox BA (1968) Basic strengthening mechanisms in refractory metals. Springer US, Boston

38. Cao Y, Shin YC, Wu B (2010) Parametric study on single shot and overlapping laser shock peening on various metals via modeling and experiments. J Manuf Sci Eng 132(6):061010